

Constraints from Λ hypernuclei on the ΛNN content of the Λ -nucleus potential

E. Friedman, A. Gal*

Racah Institute of Physics, The Hebrew University, Jerusalem 91904, Israel

Abstract

A depth of $D_\Lambda \approx -28$ MeV for the Λ -nucleus potential was confirmed in 1988 by studying Λ binding energies deduced from (π^+, K^+) spectra measured across the periodic table. Modern two-body hyperon-nucleon interaction models require additional interaction terms, most likely ΛNN three-body terms, to reproduce D_Λ . Here we apply a suitably constructed Λ -nucleus density dependent optical potential to binding energy calculations of observed $1s_\Lambda$ and $1p_\Lambda$ states in the mass range $12 \leq A \leq 208$. The resulting ΛNN contribution to D_Λ , about 14 MeV repulsion at symmetric nuclear matter density $\rho_0 = 0.17 \text{ fm}^{-3}$, makes D_Λ increasingly repulsive at $\rho \gtrsim 3\rho_0$, leading possibly to little or no Λ hyperon content of neutron-star matter. This suggests in some models a stiff equation of state that may support two solar-mass neutron stars.

Keywords: hyperon strong interactions; optical potentials; Λ hypernuclei.

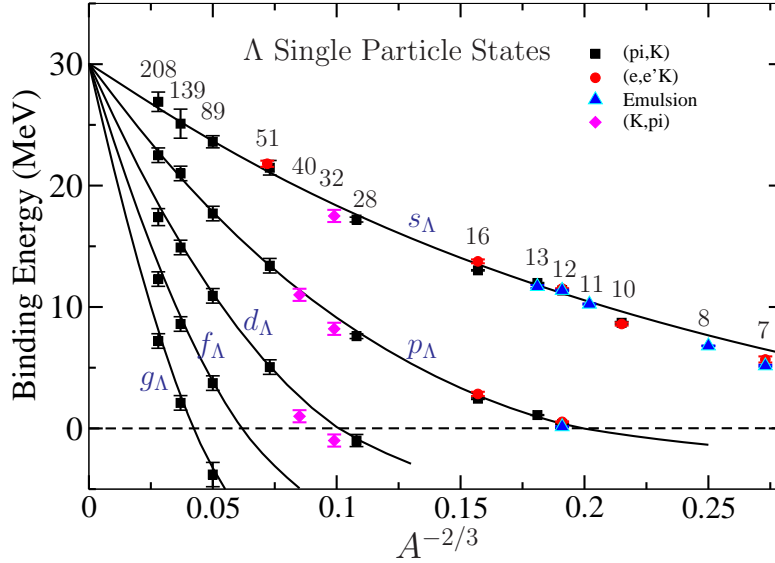
1. Introduction

The Λ -nucleus potential depth provides an important constraint in ongoing attempts to resolve the ‘hyperon puzzle’, i.e., whether or not dense neutron-star matter contains hyperons, primarily Λ s besides nucleons [1]. Fig. 1 presents compilation of most of the known Λ hypernuclear binding energies (B_Λ) across the periodic table, fitted by a three-parameter Woods-Saxon (WS) attractive potential. As $A \rightarrow \infty$, a limiting value of $B_\Lambda^{\text{exp}}(A) \rightarrow 30$ MeV is obtained. This updates the value 28 MeV from the 1988 first theoretical analysis [2] of the BNL-AGS (π^+, K^+) data [4], and

*corresponding author: Avraham Gal, avragal@savion.huji.ac.il

27 ± 3 MeV [5] 27.2 ± 1.3 MeV [6] from earlier mid 1960s observations of π^- decays of heavy spallation hypernuclei formed in silver and bromine emulsions. Interestingly, studies of density dependent Λ -nuclear optical potentials $V_\Lambda(\rho)$ in Ref. [2] conclude that a ρ^2 term motivated by three-body ΛNN interactions provides a large repulsive (positive) contribution to the Λ -nuclear potential depth D_Λ at nuclear-matter density ρ_0 : $D_\Lambda^{(3)} \approx 30$ MeV. This repulsive component of D_Λ is more than just compensated at ρ_0 by a roughly twice larger attractive depth value, $D_\Lambda^{(2)} \approx -60$ MeV, motivated by a two-body ΛN interaction. Note that $D_\Lambda = D_\Lambda^{(2)} + D_\Lambda^{(3)}$ is defined as $V_\Lambda(\rho_0)$ in the limit $A \rightarrow \infty$ at a given nuclear-matter density ρ_0 , with a value 0.17 fm^{-3} assumed here.

Update: Millener, Dover, Gal PRC 38, 2700 (1988)



Woods-Saxon $V = 30.05$ MeV, $r = 1.165$ fm, $a = 0.6$ fm

Figure 1: Compilation of Λ binding energies in ${}^7_\Lambda\text{Li}$ to ${}^{208}_\Lambda\text{Pb}$ from various sources, and as calculated using a three-parameter WS potential [2]. Figure adapted from Ref. [3].

Most hyperon-nucleon potential models overbind Λ hypernuclei, yielding values of $D_\Lambda^{(2)}$ deeper than -30 MeV. Whereas such overbinding amounts to

only few MeV in the often used Nijmegen soft-core model versions NSC97e,f [7] it is considerably stronger, by more than 10 MeV, in the recent Nijmegen extended soft-core model ESC16 [8]. A similar overbinding arises at leading order in chiral effective field theory (χ EFT) [9]. The situation at next-to leading order (NLO) is less clear owing to a strong dependence of $D_{\Lambda}^{(2)}$ on the momentum cutoff scale λ [10]. At $\lambda=500$ MeV/c, however, it is found in Ref. [11] that both versions NLO13 [12] and NLO19 [13] overbind by a few MeV. Finally, recent Quantum Monte Carlo (QMC) calculations [14, 15], using a $\Lambda N + \Lambda NN$ interaction model designed to bind correctly ${}^5_{\Lambda}\text{He}$, result in a strongly attractive $D_{\Lambda}^{(2)}$ of order -100 MeV and a correspondingly large repulsive (positive) $D_{\Lambda}^{(3)}$, reproducing the overall potential depth $D_{\Lambda} \approx -30$ MeV.

Introducing repulsive three-body ΛNN interactions goes beyond just providing solution of the overbinding problem: as nuclear density is increased beyond nuclear matter density ρ_0 , the balance between attractive $D_{\Lambda}^{(2)}$ and repulsive $D_{\Lambda}^{(3)}$ tilts towards the latter. This results in nearly total expulsion of Λ hyperons from neutron-star matter, suggesting an equation of state (EoS) sufficiently stiff to support two solar-mass neutron stars, thereby providing a possible solution to the ‘hyperon puzzle’. The larger $D_{\Lambda}^{(3)}$ is, the more likely it is a solution [16, 17]. However, there is no guarantee that three-body ΛNN interactions are universally repulsive. For a recent discussion of this problem within an SU(3) ‘decuplet dominance’ approach practised in modern χ EFT studies at NLO, see Ref. [11].

Our aim in the present phenomenological study is to check to what extent properly chosen Λ hypernuclear binding energy data, with minimal extra assumptions, imply positive values of $D_{\Lambda}^{(3)}$, and how large it is. To do so, we follow the optical potential approach applied by Dover-Hüfner-Lemmer to pions in nuclear matter [18]. Applied to the Λ -nucleus system, it provides expansion in powers of the nuclear density $\rho(r)$, consisting of a linear term induced by a two-body ΛN interaction plus two higher-power density terms: (i) a long-range Pauli correlations term starting at $\rho^{4/3}$, and (ii) a short-range NN interaction term dominated in the present context by three-body ΛNN interactions, starting at ρ^2 . As will become clear below, the contribution of the Pauli correlations term is non negligible, propagating to higher powers of density terms than just $\rho^{4/3}$, such as the ρ^2 ΛNN interaction term. This explains why the value derived here, $D_{\Lambda}^{(3)} = (13.9 \pm 1.4)$ MeV, differs from any of those suggested earlier in Ref. [2] and in Skyrme Hartree Fock studies

[19] where Pauli correlations apparently were disregarded. Our value of $D_\Lambda^{(3)}$ strongly disagrees with the much larger value inferred in QMC calculations [15]. We comment on this discrepancy below.

The paper is organized as follows. In Sect. 2 we present the form of the optical potential $V_\Lambda^{\text{opt}}(\rho)$ used to evaluate B_Λ values across the periodic table. The choice of B_Λ^{exp} data and nuclear densities ρ , providing input to the present B_Λ calculations, is briefly discussed. Results are given and discussed in Sect. 3, and concluding remarks are made in Sect. 4.

2. Optical Potential Methodology and Input

The optical potential employed in this work, $V_\Lambda^{\text{opt}}(\rho) = V_\Lambda^{(2)}(\rho) + V_\Lambda^{(3)}(\rho)$, consists of terms representing two-body ΛN and three-body ΛNN interactions, respectively:

$$V_\Lambda^{(2)}(\rho) = -\frac{4\pi}{2\mu_\Lambda} f_A C_{\text{Pauli}}(\rho) b_0 \rho, \quad (1)$$

$$V_\Lambda^{(3)}(\rho) = +\frac{4\pi}{2\mu_\Lambda} f_A B_0 \frac{\rho^2}{\rho_0}, \quad (2)$$

with b_0 and B_0 strength parameters in units of fm ($\hbar = c = 1$). In these expressions, A is the mass number of the nuclear core, ρ is a nuclear density normalized to A , $\rho_0 = 0.17 \text{ fm}^{-3}$ stands for nuclear matter density, μ_Λ is the Λ -nucleus reduced mass and f_A is a kinematical factor transforming b_0 from the ΛN c.m. system to the Λ -nucleus c.m. system:

$$f_A = 1 + \frac{A-1}{A} \frac{\mu_\Lambda}{m_N}. \quad (3)$$

This form of f_A coincides with the way it is used for $V_\Lambda^{(2)}$ in atomic/nuclear hadron-nucleus bound-state problems [20] and its A dependence provides good approximation for $V_\Lambda^{(3)}$. Next in Eq. (1) is the density dependent Pauli correlation function $C_{\text{Pauli}}(\rho)$:

$$C_{\text{Pauli}}(\rho) = (1 + \alpha_P \frac{3k_F}{2\pi} f_A b_0)^{-1}, \quad (4)$$

with Fermi momentum $k_F = (3\pi^2\rho/2)^{1/3}$. The parameter α_P in Eq. (4) switches off ($\alpha_P=0$) or on ($\alpha_P=1$) Pauli correlations in a form suggested in

Ref. [21] and practised in K^- atoms studies [22]. Following Ref. [23] we approximated f_A in $C_{\text{Pauli}}(\rho)$ by $f_{A \rightarrow \infty}$. As shown below, including $C_{\text{Pauli}}(\rho)$ in $V_{\Lambda}^{(2)}$ affects strongly the balance between the derived potential depths $D_{\Lambda}^{(2)}$ and $D_{\Lambda}^{(3)}$. However, introducing it also in $V_{\Lambda}^{(3)}$ is found to make little difference, which is why it is skipped in Eq. (2). Finally we note that the low-density limit of V_{Λ}^{opt} requires according to Ref. [18] that b_0 is identified with the c.m. ΛN spin-averaged scattering length (positive here). We now specify the B_{Λ} data dealt with in the present analysis and the nuclear densities $\rho(r)$ used for constructing the density dependent optical potential $V_{\Lambda}(\rho)$, Eqs. (1,2).

2.1. B_{Λ} Data

The present work does not attempt to reproduce the full range of B_{Λ} data shown in Fig. 1. It is limited to $1s_{\Lambda}$ and $1p_{\Lambda}$ states. We fit to such states in *one* of the nuclear p -shell hypernuclei where the $1s_{\Lambda}$ state is bound by over 10 MeV, while the $1p_{\Lambda}$ state has just become bound. This helps to resolve the density dependence of V_{Λ}^{opt} by setting a good balance between its two components, $V_{\Lambda}^{(2)}(\rho)$ and $V_{\Lambda}^{(3)}(\rho)$, and follow it throughout the periodic table up to the heaviest hypernucleus of ${}^{208}_{\Lambda}\text{Pb}$ marked in Fig. 1. Among the relevant $A = 12, 13, 16$ p -shell hypernuclei, we chose to fit the ${}^{16}_{\Lambda}\text{N}$ precise $B_{\Lambda}^{\text{exp}}(1s, 1p)$ values, partly because of the extremely simple $1p$ proton hole structure of its nuclear core which removes most of the uncertainty arising from spin-dependent residual ΛN interactions [24].

The $B_{\Lambda}^{\text{exp}}(1s, 1p)$ values considered in the present work are those shown in Fig. 1 for $12 \leq A \leq 208$, as listed in Table IV of Ref. [3] and remarked on in the related text. Most of these values are from (π^+, K^+) reactions. Older (K^-, π^-) data for ${}^{32}_{\Lambda}\text{S}$ were included to enhance the only (π^+, K^+) data available in the $2s$ - $1d$ shell, for ${}^{28}_{\Lambda}\text{Si}$. For $A = 12, 16$ we used the more precise $B_{\Lambda}^{\text{exp}}(1s, 1p)$ values extracted in $(e, e'K^+)$ reactions at JLab [25], ${}^{12}_{\Lambda}\text{B}$ in preference to ${}^{12}_{\Lambda}\text{C}$ and ${}^{16}_{\Lambda}\text{N}$ instead of ${}^{16}_{\Lambda}\text{O}$. Whereas the ${}^{12}_{\Lambda}\text{C}$ values agree with the ${}^{12}_{\Lambda}\text{B}$ respective values within measurement uncertainties, this is not the case for the $A = 16$ species where the $1s$ values differ by 0.8 ± 0.3 MeV. However, a more recent $(K_{\text{stop}}^-, \pi^-)$ measurement on ${}^{16}\text{O}$ reports $B_{\Lambda}^{1s}({}^{16}_{\Lambda}\text{N}) = 13.4 \pm 0.4$ MeV [26] consistently within its uncertainty range with the $(e, e'K^+)$ value $B_{\Lambda}^{1s}({}^{16}_{\Lambda}\text{N}) = 13.76 \pm 0.16$ MeV [27] used here. We comment below on the sensitivity of our calculational results to this difference.

2.2. Nuclear Densities

In optical model applications similar to the one adopted here, it is crucial to ensure that the radial extent of the densities, e.g., their r.m.s. radii follow closely values derived from experiment. With $\rho(r) = \rho_p(r) + \rho_n(r)$, the sum of proton and neutron density distributions, respectively, we relate the proton densities to the corresponding charge densities where the finite size of the proton charge and recoil effects are included. This approach is equivalent to assigning some finite range to the Λ -nucleon interaction. For the lightest elements in our database we used harmonic-oscillator type densities, assuming the same radial parameters also for the corresponding neutron densities [28]. For species beyond the nuclear $1p$ shell we used two-parameter and three-parameter Fermi distributions normalized to Z for protons and $N = A - Z$ for neutrons, derived from nuclear charge distributions assembled in Ref. [29]. For medium-weight and heavy nuclei, the r.m.s. radii of neutron density distributions assume larger values than those for proton density distributions, as practiced in analyses of exotic atoms [20]. Furthermore, once neutrons occupy single-nucleon orbits beyond those occupied by protons, it is useful to represent the nuclear density $\rho(r)$ as

$$\rho(r) = \rho_{\text{core}}(r) + \rho_{\text{excess}}(r), \quad (5)$$

where ρ_{core} refers to the Z protons plus the charge symmetric Z neutrons occupying the same nuclear ‘core’ orbits, and ρ_{excess} refers to the $(N - Z)$ ‘excess’ neutrons associated with the nuclear periphery.

3. Results and Discussion

Λ -nuclear potential depths $D_{\Lambda}^{(2)}$, $D_{\Lambda}^{(3)}$ from our optical-potential calculations, and their sum D_{Λ} , are listed in Table 1 for several choices of V_{Λ}^{opt} models specified in detail below. Calculated $1s_{\Lambda}$ and $1p_{\Lambda}$ binding energies in hypernuclei from ${}^{12}_{\Lambda}\text{B}$ to ${}^{208}_{\Lambda}\text{Pb}$ are shown in Fig. 2 for models P,Q, and in Fig. 3 for models X,Y, in comparison to $B_{\Lambda}^{\text{exp}}(1s, 1p)$ data.

In Model P, the optical potential $V_{\Lambda}(\rho)$ consists of just a linear-density $V_{\Lambda}^{(2)}(\rho)$ term, disregarding Pauli correlations ($\alpha_P=0$). Its only strength parameter b_0 is fitted to $B_{\Lambda}^{1s}({}^{16}_{\Lambda}\text{N})=13.76\pm 0.16$ MeV. This and other $B_{\Lambda}(1s, 1p)$ values calculated in Model P are plotted in the upper part of Fig. 2. The model does well for $1s_{\Lambda}$ states below ${}^{16}_{\Lambda}\text{N}$ and then in ${}^{208}_{\Lambda}\text{Pb}$, but not in between. For $1p_{\Lambda}$ states it misses seriously the measured binding energies below

Table 1: Strength parameters: (i) b_0, B_0 (fm), Eqs. (1,2), in models P,Q,X,Y of the present work, or (ii) c_0, C_0 ($\text{MeV}\cdot\text{fm}^3$, $\text{MeV}\cdot\text{fm}^6$) for $V_\Lambda(\rho) = -c_0\rho + C_0\rho^2$ from Ref. [2]; plus their respective potential depths $D_\Lambda^{(2)}$, $D_\Lambda^{(3)}$ and sum D_Λ (MeV) at nuclear matter density $\rho_0 = 0.17 \text{ fm}^{-3}$. Pauli correlations are switched off (on) using $\alpha_P = 0$ (1) in Eq. (4).

Model	α_P	b_0 or c_0	B_0 or C_0	$D_\Lambda^{(2)}$	$D_\Lambda^{(3)}$	D_Λ
P	0	0.418	–	–34.1	–	–34.1
P'	1	0.908	–	–32.3	–	–32.3
Q	0	0.706	0.370	–57.6	30.2	–27.4
MDG [2]	0	340.0	1087.5	–57.8	31.4	–26.4
X,Y	1	1.85	0.170	–41.6	13.9	–27.7

$^{28}_\Lambda\text{Si}$, while doing fairly well in heavier species. The potential depth D_Λ (here at $\rho_0 = 0.17 \text{ fm}^{-3}$) associated with Model P is -34.1 MeV (-32.1 MeV at $\rho_0 = 0.16 \text{ fm}^{-3}$), decreasing in size to -32.3 MeV upon switching on Pauli correlations ($\alpha_P=1$, Model P' in the table). The roughly 5% decrease in size of D_Λ is comparable to the 10% decrease in size of D_Ξ found recently for Ξ^- hyperons [23].

In Model Q, a $V_\Lambda^{(3)}(\rho) \rho^2$ component is added to the $V_\Lambda^{(2)}(\rho)$ linear-density component, but still with no Pauli correlations ($\alpha_P=0$). The two strength parameters b_0, B_0 are obtained by fitting to $B_\Lambda^{1s}(^{16}_\Lambda\text{N})=13.76\pm 0.16 \text{ MeV}$ and $B_\Lambda^{1p}(^{16}_\Lambda\text{N})=2.84\pm 0.18 \text{ MeV}$. These and other $B_\Lambda(1s, 1p)$ values calculated in Model Q are plotted in the lower part of Fig. 2. The overall fit quality is a bit improved with respect of that in Model P, but some underbinding appears to develop upon increasing the mass number A , noticed clearly in the three heaviest $1s_\Lambda$ and two heaviest $1p_\Lambda$ states. The resulting Λ potential depth $D_\Lambda = -27.4 \text{ MeV}$ reflects a sizable cancellation between a strongly attractive two-body potential depth $D_\Lambda^{(2)}$ and a strongly repulsive three-body potential depth $D_\Lambda^{(3)}$ listed in Table 1. Interestingly, these two partial depths almost coincide with those listed in the following line of the table marked Model MDG after Ref. [2].

Pauli correlations are switched on ($\alpha_P=1$) in Models X and Y. Model X uses the same densities $\rho(r)$ and $\rho^2(r)$ used in Models P,Q. We note in Table 1 the steady increase of the fitted two-body strength parameter b_0 by roughly factor of two going from Model P to P', where Pauli correlations were switched on, or to Q where a three-body $\rho^2(r)$ term was introduced, and finally by roughly factor of four in Model X upon including both Pauli cor-

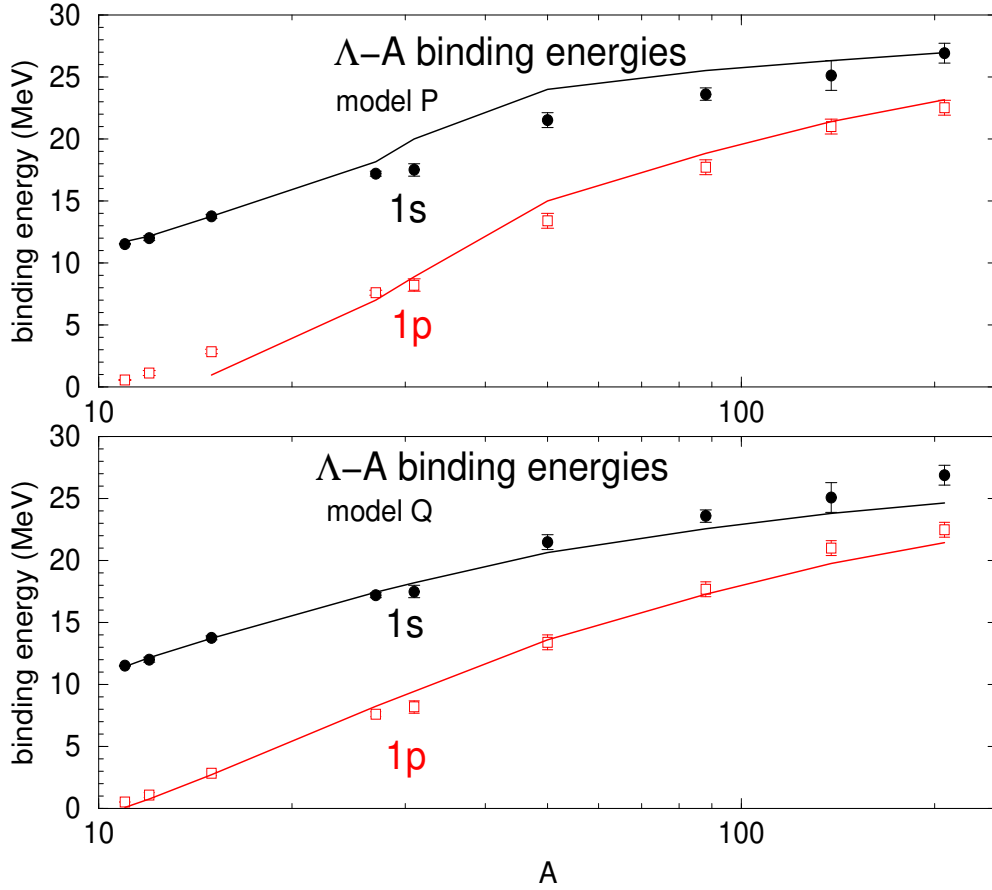


Figure 2: $B_{\Lambda}^{1s,1p}(A)$ values in Models P (upper) Q (lower) across the periodic table, see text. Data points, including uncertainties, are taken from Table IV of Ref. [3]. Continuous lines connect calculated values.

relations and a three-body term. The fitted value in Model X, $b_0 = 1.85$ fm, is close to the spin averaged value of the ΛN scattering length suggested by experiments (e.g., 1.65 fm [30] or 1.78 fm [31]). This indicates that once both Pauli correlations and a three-body term are taken into account, the present optical potential form satisfies approximately its $\rho \rightarrow 0$ constraint. We also note that the fitted three-body strength parameter B_0 is down by more than factor of two from its fitted value in Model Q where Pauli correlations were disregarded. It is a simple matter to check that the density expansion of $C_{\text{Pauli}}(\rho)$ produces repulsion at order ρ^2 which substitutes then for part of

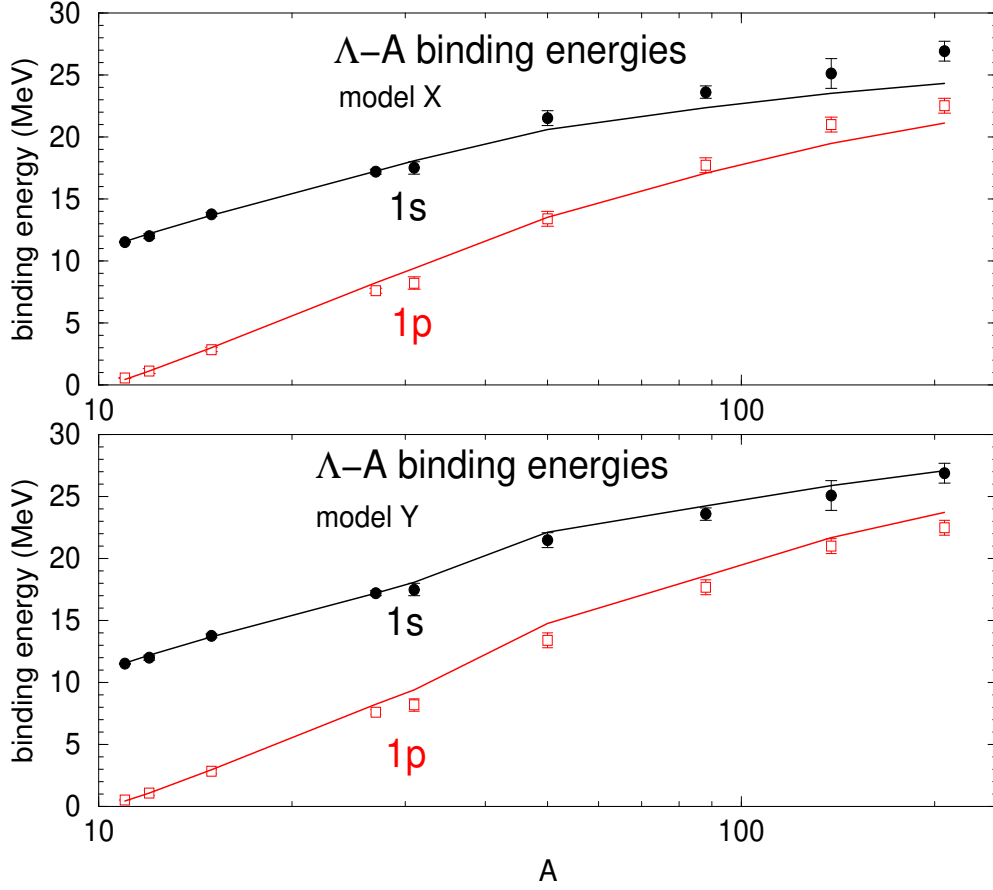


Figure 3: $B_{\Lambda}^{1s,1p}(A)$ values in Models X (upper) Y (lower) across the periodic table, see text. Data points, including uncertainties, are taken from Table IV of Ref. [3]. Continuous lines connect calculated values.

the value of B_0 in Model Q. Yet, Model X is unsatisfactory with respect to its calculated $B_{\Lambda}(1s, 1p)$ values plotted in the upper part of Fig. 3. The slight $1s_{\Lambda}$ underbinding observed in Model Q for $A \gtrsim 90$ has become more pronounced, beginning already with $A \gtrsim 50$, joined there now by considerable $1p_{\Lambda}$ underbinding. To address these shortcomings we introduce Model Y.

Model Y differs from Model X by the form of ρ^2 used in nuclei where excess neutrons occupy shell-model orbits higher than those occupied by protons. This situation occurs in Fig. 3 for the four hypernuclei with $A \gtrsim 50$. We recall

that the ΛNN interaction underlying the $V_\Lambda^{(3)} \rho^2$ term arises in χ EFT models [11] from intermediate ΣNN and $\Sigma^*(1385)NN$ states, yielding a $\vec{\tau}_1 \cdot \vec{\tau}_2$ isospin factor for the two nucleons [32, 33]. Extending the discussion in Ref. [34], it can be shown that direct three-body ΛNN contributions involving one ‘core’ nucleon and one ‘excess’ nucleon vanish upon summing on the $T=0$ ‘core’ closed-shell nucleons, while their exchange partners renormalize the two-body ΛN interaction. To modify ρ^2 accordingly, we discard the bilinear term $\rho_{\text{core}}\rho_{\text{excess}}$, thereby replacing ρ^2 in $V_\Lambda^{(3)}$, Eq. (2), by

$$\rho_{\text{core}}^2 + \rho_{\text{excess}}^2 \rightarrow (2\rho_p)^2 + (\rho_n - \rho_p)^2 \quad (6)$$

in terms of the available densities ρ_p and ρ_n . This prescription does not impact the five hypernuclei lighter than ^{40}Ca in Fig. 3, and it appears to work well as seen by the significant improvement in the $B_\Lambda(1s)$ values calculated beyond ^{40}Ca in Model Y, lower part of Fig. 3, compared to those in Model X in the upper part of the figure.

As a simple check on the Model Y results exhibited in Fig. 3, we apply a scaling-factor fraction F to the ρ^2 term of Model X,

$$F = \frac{(2Z)^2 + (N - Z)^2}{A^2}. \quad (7)$$

This fraction is the reduced ρ^2 volume integral of a core of Z protons and their charge symmetric Z neutrons, and excess of $(N - Z)$ neutrons, out of the A nucleons. The resulting B_Λ values in this simplified model indeed agree closely with those in Model Y shown in the lower part of the figure. Interestingly, if this scaling factor F is applied in Model Q where $D_\Lambda^{(3)}$ is more than twice larger than in Model Y (see Table 1), Λ single-particle states in the four heaviest hypernuclei shown in the lower panel of Fig. 2 become substantially overbound, e.g. $B_\Lambda^{1s}(^{208}\text{Pb})=32.0$ MeV. This demonstrates the importance of including Pauli correlations in the $V_\Lambda^{(2)}$ component of the Λ -nucleus optical potential.

Potential depth values derived in models discussed above are listed in Table 1. Model Y in particular gives $D_\Lambda^{(2)} = -41.6$ MeV, $D_\Lambda^{(3)} = 13.9$ MeV. To estimate uncertainties, we act as follows: (i) decreasing the input value of $B_\Lambda^{1s}(^{16}\text{N})$ fitted to by 0.2 MeV, thereby getting halfway to the central value of $B_\Lambda^{1s}(^{16}\text{O})=13.4\pm 0.4$ MeV for ^{16}O [26] the charge symmetric partner of ^{16}N , results in approximately 10% larger value of $D_\Lambda^{(3)}$, and (ii) applying Pauli correlations to $V_\Lambda^{(3)}$ too reduces $D_\Lambda^{(3)}$ roughly by 10%. In both cases

$D_{\Lambda}^{(2)}$ increases moderately by $\lesssim 1$ MeV. On the other hand, $D_{\Lambda}^{(2)}$ decreases by 1.7 MeV once the A dependence of f_A , neglected in our present use of $C_{\text{Pauli}}(\rho)$ Eq. (4), is restored. Considering these uncertainties, our final values are (in MeV)

$$D_{\Lambda}^{(2)} = -(40.6 \pm 1.0), \quad D_{\Lambda}^{(3)} = (13.9 \pm 1.4), \quad (8)$$

and $D_{\Lambda} = -26.7 \pm 1.7$ MeV.

The $D_{\Lambda}^{(2)}$ and $D_{\Lambda}^{(3)}$ values in Eq. (8) are considerably lower than those deduced in QMC calculations [14, 15]. Note that the QMC nuclear densities $\rho_{\text{QMC}}(r)$ are much too compact with respect to our realistic densities, with nucleon r.m.s. radii $r_N(\text{QMC})$ only $\sim 80\%$ of the known r.m.s. charge radii in ^{16}O and ^{40}Ca [35]. Since ρ scales as r_N^{-3} , applying it to the density dependence of our V_{Λ}^{opt} would transform $D_{\Lambda}^{(2)}$ and $D_{\Lambda}^{(3)}$ of Eq. (8) to $D_{\Lambda}^{(2)}(\text{QMC}) = -79.3 \pm 2.0$ MeV and $D_{\Lambda}^{(3)}(\text{QMC}) = 53.0 \pm 5.3$ MeV, their sum $D_{\Lambda}(\text{QMC}) = -26.3 \pm 5.7$ MeV agreeing within uncertainties with ours. Other factors such as the choice of fitted B_{Λ} values may contribute to increase further the size of these QMC partial depth values to come closer to as large sizes as of $\mathcal{O}(100)$ MeV reached in these works.

4. Concluding Remarks

In summary, we have presented a straightforward optical-potential analysis of $1s_{\Lambda}$ and $1p_{\Lambda}$ binding energies across the periodic table, $12 \leq A \leq 208$, based on nuclear densities constrained by charge r.m.s. radii. The potential is parameterized by constants b_0 and B_0 in front of two-body ΛN and three-body ΛNN interaction terms. These parameters were fitted to precise $B_{\Lambda}^{\text{exp}}(1s, 1p)$ values in $^{16}_{\Lambda}\text{N}$ and then used to evaluate $B_{\Lambda}(1s, 1p)$ values in the other hypernuclei considered here. Pauli correlations were found essential to establish a correct balance between b_0 and B_0 , as judged by b_0 coming out in the final Model Y analysis close to the value of the ΛN spin-averaged s -wave scattering length. Good agreement was reached in this model between the calculated $B_{\Lambda}^{1s, 1p}$ values and their corresponding B_{Λ}^{exp} values; see Fig. 3. Although values of ℓ_{Λ} other than $1s_{\Lambda}$ and $1p_{\Lambda}$ were disregarded, we checked that $B_{\Lambda}^{1d, 1f, 1g}(^{208}_{\Lambda}\text{Pb})$ values calculated in Model Y come out reasonably well within 1-2 error bars of the experimental values shown in Fig. 1.

The potential depth $D_{\Lambda}^{(3)}$ derived here, Eq. (8), suggests that in symmetric nuclear matter the Λ -nucleus potential becomes repulsive near three times

nuclear-matter density ρ_0 . Our derived depth $D_\Lambda^{(3)}$ is larger by a few MeV than the one yielding $\mu(\Lambda) > \mu(n)$ for Λ and neutron chemical potentials in purely neutron matter under a ‘decuplet dominance’ construction for the underlying ΛNN interaction terms within a χ EFT(NLO) model [11]. This suggests that the strength of the corresponding repulsive $V_\Lambda^{(3)}$ optical potential component, as constrained in the present work by data, is sufficient to prevent Λ hyperons from playing active role in neutron-star matter, thereby enabling a stiff EoS that supports two solar-mass neutron stars.

Acknowledgments

We gratefully acknowledge useful remarks by J. Mareš, D.J. Millener, H. Tamura, I. Vidaña and W. Weise. A preliminary report of the present work was presented at the HYP2022 International Conference in Prague [36] as part of a project funded by the European Union’s Horizon 2020 research & innovation programme, grant agreement 824093.

References

- [1] L Tolos, L. Fabbietti, Prog. Part. Nucl. Phys. 112 (2020) 103770, and references to earlier work cited therein.
- [2] D.J. Millener, C.B. Dover, A. Gal, Phys. Rev. C 38 (1988) 2700.
- [3] A. Gal, E.V. Hungerford, D.J. Millener, Rev. Mod. Phys. 88 (2016) 035004.
- [4] P. Pile, et al., Phys. Rev. Lett. 66 (1991) 2585.
- [5] J.P. Lagnaux, et al., Nucl. Phys. 60 (1964) 97.
- [6] J. Lemonne, et al., Phys. Lett. 18 (1965) 354.
- [7] Th.A. Rijken, V.G.J. Stoks, Y. Yamamoto, Phys. Rev. C **59** (1999) 21.
- [8] M.M. Nagels, Th.A. Rijken, Y. Yamamoto, Phys. Rev. C 99 (2019) 044003.
- [9] H. Polinder, J. Haidenbauer, U.-G. Meißner, Nucl. Phys. A 779 (2006) 244.

- [10] J. Haidenbauer, I. Vidaña, Eur. Phys. J. A 56 (2020) 55.
- [11] D. Gerstung, N. Kaiser, W. Weise, Eur. Phys. J. A 56 (2020) 175, and references cited therein to earlier works on ΛNN interactions in χ EFT.
- [12] J. Haidenbauer, S. Petschauer, N. Kaiser, U.-G. Meißner, A. Nogga, W. Weise, Nucl. Phys. A 915 (2013) 24.
- [13] J. Haidenbauer, U.-G. Meißner, A. Nogga, Eur. Phys. J. A 56 (2020) 91.
- [14] D. Lonardoni, S. Gandolfi, F. Pederiva, Phys. Rev. C 87 (2013) 041303(R).
- [15] D. Lonardoni, F. Pederiva, S. Gandolfi, Phys. Rev. C 89 (2014) 014314.
- [16] D. Lonardoni, A. Lovato, S. Gandolfi, F. Pederiva, Phys. Rev. Lett. 114 (2015) 092301.
- [17] D. Logoteta, I. Vidaña, I. Bombaci, Eur. Phys. J. A 55 (2019) 207.
- [18] C.B. Dover, J. Hüfner, R.H. Lemmer, Ann. Phys. (NY) 66 (1971) 248.
- [19] H.-J. Schulze, E. Hiyama, Phys. Rev. C 90 (2014) 047301, and past SHF work cited therein.
- [20] E. Friedman, A. Gal, Phys. Rep. 452 (2007) 89.
- [21] T. Waas, M. Rho, W. Weise, Nucl. Phys. A 617 (1997) 449.
- [22] E. Friedman, A. Gal, Nucl. Phys. A 959 (2017) 66, and references to past work on K^- atoms cited therein.
- [23] E. Friedman, A. Gal, Phys. Lett. B 820 (2021) 136555.
- [24] D.J. Millener, Nucl. Phys. A 804 (2008) 84, 881 (2012) 298, 914 (2013) 109.
- [25] F. Garibaldi, et al. (Jefferson Lab Hall A Collaboration), Phys. Rev. C 99 (2019) 054309.
- [26] M. Agnello, et al. (FINUDA Collaboration), Phys. Lett. B 698 (2011) 219.

- [27] F. Cusanno, et al. (Jefferson Lab Hall A Collaboration), *Phys. Rev. Lett.* 103 (2009) 202501.
- [28] L.R.B. Elton, *Nuclear Sizes* (Oxford University Press, Oxford, 1961).
- [29] I. Angeli, K.P. Marinova, *At. Data Nucl. Data Tables* 99 (2013) 69.
- [30] G. Alexander, et al., *Phys. Rev.* 173 (1968) 1452.
- [31] A. Budzanowski, et al. (HIRES Collaboration), *Phys. Lett. B* 687 (2010) 31.
- [32] R. Spitzer, *Phys. Rev.* 110 (1958) 1190.
- [33] R.K. Bhaduri, B.A. Loiseau, Y. Nogami, *Ann. Phys. (NY)* 44 (1967) 57.
- [34] A. Gal, J.M. Soper, R.H. Dalitz, *Ann. Phys. (NY)* 63 (1971) 53, in particular Sect. 4.
- [35] D. Lonardonì, Ph.D. thesis submitted to the University of Trento, Italy, arXiv:1311.6672; see Table 4.7.
- [36] E. Friedman, A. Gal, *EPJ Web Conf.* 271 (2022) 06002.